

Making Atomic-Level Magnetism Tunable with Light at Room Temperature

V.O. Jimenez^{1,*}, Y.T.H. Pham¹, D. Zhou², M.Z. Liu², F.A. Nugera¹, V. Kalappattil¹, T. Eggers¹,
K. Hoang³, D.L. Duong⁴, M. Terrones², H.R. Gutiérrez¹, and M.H. Phan^{1,*}

¹ Department of Physics, University of South Florida, Tampa, FL 33620, USA

² Department of Physics, The Pennsylvania State University, University Park, PA 16802, USA

³ Center for Computationally Assisted Science and Technology and Department of Physics, North
Dakota State University, Fargo, ND 58108, USA

⁴ Department of Physics, Montana State University, Bozeman, MT 59717, USA

The capacity to manipulate magnetization in two-dimensional dilute magnetic semiconductors (2D-DMSs) using light, specifically in magnetically doped transition metal dichalcogenide (TMD) monolayers (M -doped TX_2 , where $M = V, Fe, Cr$; $T = W, Mo$; $X = S, Se, Te$), may lead to innovative applications in spintronics, spin-caloritronics, valleytronics, and quantum computation. This Perspective paper explores the mediation of magnetization by light under ambient conditions in 2D-TMD DMSs and heterostructures. By combining magneto-LC resonance (MLCR) experiments with density functional theory (DFT) calculations, we show that the magnetization can be enhanced using light in V-doped TMD monolayers (e.g., V-WS₂, V-WSe₂, V-MoS₂). This phenomenon is attributed to excess holes in the conduction and valence bands, as well as carriers trapped in magnetic doping states, which together mediate the magnetization of the semiconducting layer. In 2D-TMD heterostructures such as VSe₂/WS₂ and VSe₂/MoS₂, we demonstrate the significance of proximity, charge-transfer, and confinement effects in amplifying light-mediated magnetism. This effect is attributed to photon absorption at the TMD layer (e.g., WS₂, MoS₂) that generates electron-hole pairs mediating the magnetization of the heterostructure. These findings will encourage further research in the field

of 2D magnetism and establish a novel direction for designing 2D-TMDs and heterostructures with optically tunable magnetic functionalities, paving the way for next-generation magneto-optic nanodevices.

Keywords: 2D van der Waals magnets; Transition Metal Dichalcogenides; Heterostructures; Opto-spintronics; Spin-caloritronics; Valleytronics; Quantum Communications

***Corresponding authors:** valeryortizj@usf.edu (V.O.J); phanm@usf.edu (M.H.P)

1. Introduction

Magnetic semiconductors present an exceptional platform for the development of a new generation of highly efficient spintronic devices, including spin field-effect (SFE) transistors [1-7]. In contrast to conventional field-effect transistors that rely on electron charge, SFE transistors utilize electron spin and its alignment (up or down) within a magnetic semiconductor to encode binary information, facilitating rapid information transmission with minimal power consumption [1,4]. To diminish the size of such devices, it is crucial to reduce the dimensions of semiconductor materials [4,7-9]. As dimensions decrease, novel physical properties emerge, and new potential applications arise. However, miniaturization to the nanoscale might substantially impair their performance due to current leakage, rendering such devices inapplicable in ultrafast electronic nanodevices, particularly in supercomputers or future quantum computers [1,7]. For most magnetic semiconductors, ferromagnetic properties are largely weakened or even lost when their thickness is reduced to the atomic level or two-dimensional (2D) limit [1,2,7].

Recent advances in the domain of 2D van der Waals (vdW) magnetic materials have yielded unprecedented opportunities for exploiting atomically thin magnets [10-14] and heterostructures [15-27] with tunable magnetic, magnetoelectric, and magneto-optic properties. Among the identified 2D vdW magnets, the atomically thin intrinsic magnetic semiconductors CrI_3 and $\text{Cr}_2\text{Ge}_2\text{Te}_6$ have been extensively studied for their novel magnetoelectric, magneto-optic, and spin transport properties [10,11,28-37]. Their magnetic functionalities can also be modulated by external stimuli (electric gating, strain, light) [38-47]. Regrettably, these 2D semiconductors exhibit magnetic ordering at low temperatures (< 50 K), limiting their practical implementation. Consequently, there is a growing demand for the development of 2D magnetic semiconductors that exhibit ferromagnetic ordering at ambient temperatures, under which most electronic devices operate.



Figure 1. Perspectives of novel device applications of atomically thin magnetic transition metal dichalcogenides and their heterostructures.

Two-dimensional transition metal dichalcogenides (2D-TMDs) TX_2 ($T = W, Mo; X = S, Se, Te$) are central to numerous vital device applications such as field-effect transistors, photodetectors, photon emitters, valleytronics, and quantum computers [3,4,7,8,48,49]. Despite the presence of certain 2D-TMDs such as VSe_2 [13], $MnSe_2$ [14], and $CrSe_2$ [50], which exhibit ferromagnetic ordering near room temperature but are *metallic*, the majority of *semiconducting* 2D-TMDs including WSe_2 , WS_2 , and MoS_2 monolayers are non-magnetic or diamagnetic in nature [51]. Recent studies have shown that introducing small quantities of magnetic transition metal atoms (e.g., V, Fe, Co, Cr, Mn) can induce long-range ferromagnetic order in these 2D-TMDs at room temperature [52-73]. This approach presents a promising strategy to integrate extrinsic magnetic properties into atomically thin TMD semiconductors, giving rise to a novel class of two-dimensional dilute magnetic semiconductors

(2D-DMSs). Due to their high-quality interfaces and weakly coupled interlayer interactions, 2D-TMDs with desirable properties can be easily stacked together, creating 2D vdW heterostructures with unique properties otherwise absent in their individual components [7,77-86]. Their potential for next generation spintronic, opto-spintronic, opto-spin-caloritronic, and valleytronic device applications has been emphasized, owing to their atomically thin nature and integrated opto-electromagnetic properties [7,83-86]. Figure 1 illustrates potential applications of 2D-TMD DMSs and their heterostructures.

The true appeal of 2D-TMD DMSs for these applications stems from their magnetic tunability in response to external stimuli (electric gating, light, strain). Magnetic state tunability of a 2D-TMD can range from enhancing its magnetic moment, tuning its Curie temperature to inducing magnetism in non-magnetic materials through chemical doping [52,53], defect engineering [60], phase change or structure engineering [75,87,88], interface engineering [77-82], or applying external stimuli [56,57,89]. Among these approaches, the capacity to modulate the magnetic moments of 2D-TMDs reversibly, using external stimuli such as electric gating or light, appears to accommodate the ever-increasing demands for multifunctional sensing devices, information storage, and quantum computing technologies. Our discovery of tunable room temperature ferromagnetism in atomically thin V-doped TMD (V-WS₂, V-WSe₂, V-MoS₂) semiconductors [52,53] has provided a new possibility for controlling their magnetic and magneto-electronic properties through optical means [56,90]. By combining the light-tunable magnetism of 2D-DMSs [56,90] and the spin Seebeck effect [91], we have proposed an innovative strategy for the optic control of thermally driven spin currents across magnet/metal interfaces in spin-caloritronic devices, potentially establishing a new subfield dubbed “Opto-Spin-Caloritronics” [84]. To fully exploit the optically tunable magnetic properties of 2D-TMD DMSs and their heterostructures for spintronics, spin-caloritronics, straintronics, and

valleytronics (Fig. 1), it is essential to comprehend the underlying mechanisms of light-mediated magnetism in these 2D systems.

In this Perspective article, we demonstrate how light modulates the magnetization in 2D-TMD DMSs (V-WS₂, V-WSe₂, V-MoS₂) and associated heterostructures (VSe₂/MoS₂, VSe₂/WS₂), using an ultrasensitive magneto-LC resonance (MLCR) magnetometer. Supplemented by DFT calculations, these findings enable us to propose innovative design strategies for novel 2D-TMD DMSs and heterostructures with enhanced light-tunable magnetic functionalities suitable for modern nanodevice applications. Figure 2 presents two promising approaches for creating such 2D-TMDs and heterostructures, with their optically tunable magnetic properties discussed herein.

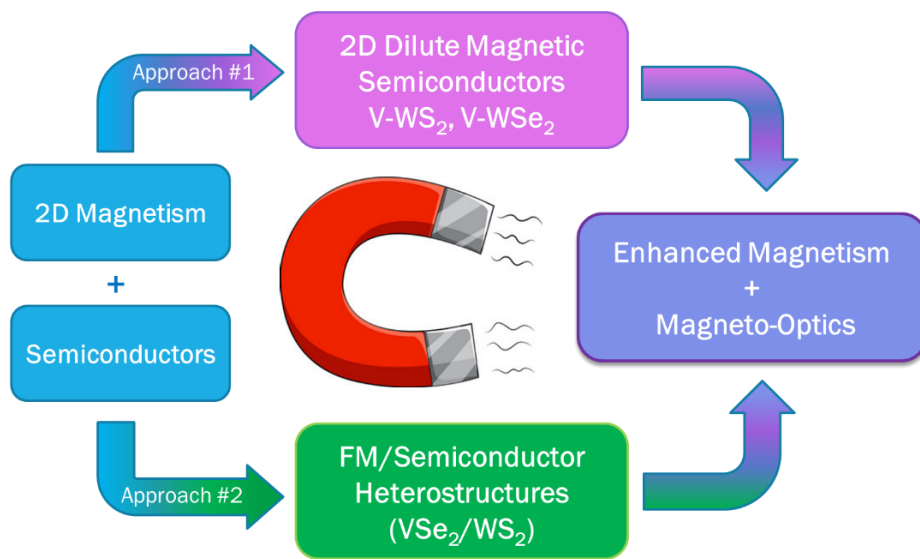


Figure 2. Approach 1: Introducing small amounts of magnetic atoms (e.g., V, Fe, Cr) into semiconducting TMD monolayers (e.g., WS₂, WSe₂, MoS₂) creates a novel class of 2D dilute magnetic semiconductors (e.g., V-WS₂, V-WSe₂, V-MoS₂). **Approach 2:** Interfacing 2D-TMD magnets (e.g., VSe₂, VS₂, MnSe₂, CrSe₂) with 2D-TMD semiconductors (e.g., WS₂, WSe₂, MoS₂) create a novel class of magneto-optic 2D van der Waals heterostructures (e.g., VSe₂/WS₂, VS₂/MoS₂, MnSe₂/WSe₂, CrSe₂/WSe₂).

The paper is structured as follows: we first introduce the MLCR magnetometry technique and then use this technique to demonstrate the light-mediated magnetism effects in the 2D-TMD DMSs and related heterostructures. We will also discuss emerging opportunities and challenges in the field of study.

2. Magneto-LC Resonance Magnetometry for Probing Light-Mediated Magnetism

As ferromagnetic signals become exceedingly weak in atomically thinned magnetic systems, probing small changes in magnetization of the material subject to external stimuli, such as light, presents a considerable challenge [39,41,43,92-103]. Superconducting quantum interference devices (SQUID) can measure the magnetization of 2D materials [52,53], but they are not well-suited for real-time measurements while simultaneously illuminating the samples with light [93]. Transport measurements on 2D materials also pose difficulties, as the size of the electrical contacts is often larger compared to the surface area of the sample [7]. Optical methods based on the magneto-optic Kerr effect (MOKE), time-resolved Faraday rotation, and reflectance magneto-circular dichroism (RMCD) have been successfully employed to characterize the light-mediated magnetic properties of 2D materials such as Fe_3GeTe_2 [92], $\text{Cr}_2\text{Ge}_2\text{Te}_6$ [40], and CrI_3 [39]. However, the use of high laser powers in these methods may cause local heating and consequently thermal instability – a significant source of noise. The limitations of these techniques necessitate the development of a new approach to measure 2D magnetization in real time as external stimuli, such as light, are applied.

To probe the light-induced magnetization of an atomically thin magnetic film, we have developed a novel magneto-LC resonance (MLCR) magnetometer with ultrahigh magnetic field sensitivity (pT regime) [56,90].

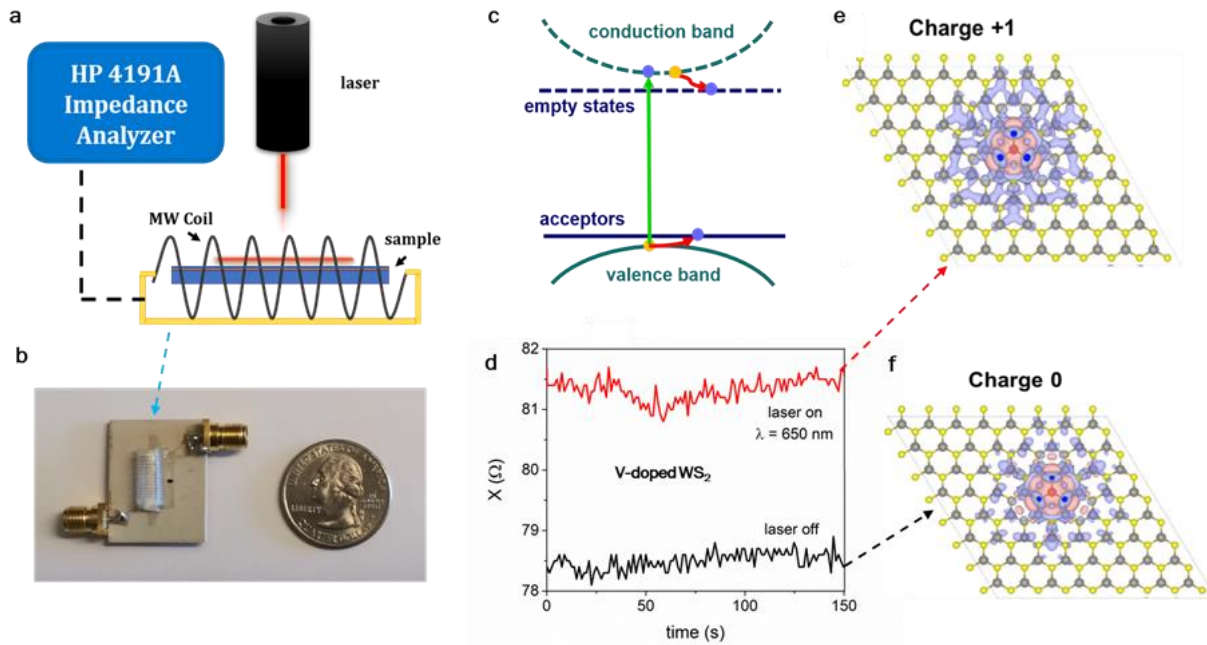


Figure 3. (a) Schematic of the MLCR measurement setup. Changes in magnetic reactance corresponding to the magnetic permeability or magnetization of a magnetic sample due to light irradiation are monitored in real time by a soft magnetic coil. The coil is mounted on a test fixture composed of a copper clad dielectric material, with its two ends soldered into the inner pin of SMA ports, as depicted in (b). (c) Schematic of the photon-induced magnetism effect when light illuminates a 2D-TMD; (d) Reactance as a function of time when the laser is off and on; The projected magnetic moment along the c-axis of the V-WS₂ monolayer upon a single hole injection (e) relative to no charge injection (f). Both MLCR experiments (d) and DFT calculations (e,f) confirm that the magnetization of the V-WS₂ monolayer increases upon light illumination.

Figure 3a presents a schematic of the light-mediated magnetization measurement system using the principle of MLCR [104,105]. The MLCR design draws inspiration from conventional magneto-inductive coils and the sensitivity of the giant magneto-impedance (GMI) effect [106], which has proven useful for detecting ultra-small magnetic fields in biosensing applications [107] and for structural health monitoring [108]. The sensor is constructed from a Co-rich soft magnetic microwire

exhibiting very high GMI ratios and magnetic field sensitivity. The melt-extracted amorphous microwire, with a nominal composition of $\text{Co}_{69.25}\text{Fe}_{4.25}\text{Si}_{13}\text{B}_{12.5}\text{Nb}_1$ and diameter of approximately $60\ \mu\text{m}$, is wound into a 15-turn, 10-mm-long coil with a 5 mm internal diameter. The coil is mounted on a test fixture made of a copper clad dielectric material (Fig. 3b). The two ends of the coil are soldered onto the inner pin of SMA ports, which are connected to a coaxial cable and terminated with a $50\text{-}\Omega$ cap. The coil is then driven by a frequency in the MHz range (~ 118 MHz, near the coil's LC resonance), and the impedance (Z), resistance (R), and reactance (X) are measured using an HP 4191A impedance analyzer.

The operating principle of the magnetic microwire coil (MMC) can be described using lumped element circuit theory. A simple model for a coil sensor is a lumped element representation of a non-ideal inductor. Winding cylindrical conductors close to each other introduces parasitic elements R_{par} and C_{par} , such that the non-ideal inductor can be represented as a series combination of an ideal inductor L and R_{par} , in parallel with C_{par} . The impedance of the coil Z_{coil} can then be written as

$$Z_{coil} = Z_{R_{par}} + Z_{C_{par}} \quad (1)$$

$$Z_{coil} = \frac{1}{\frac{1}{R_{par} + j\omega L} + \frac{1}{-j/\omega C_{par}}} \quad (2)$$

$$Z_{coil} = \frac{R_{par} + j\omega[L(1 - \omega^2 LC_{par}) - C_{par}R_{par}^2]}{(1 - \omega^2 LC_{par})^2 + (\omega C_{par}R_{par})^2} \quad (3)$$

where Z_{coil} is the impedance of the coil, ω is the angular frequency, and j is the imaginary unit. Resonance occurs when the inductive reactance (X_L) and the capacitive reactance (X_C) have equal magnitudes but differ in phase by 180 degrees. In this case, minimal current flows through the wire, the impedance of the coil becomes very large, and self-resonance is achieved. This resonance frequency is given by:

$$f_0 = \frac{\sqrt{1 - (R_{par}^2 C_{par} / L)}}{2\pi\sqrt{LC_{par}}} \quad (4)$$

The reactance of the coil is of particular interest to utilize the coil for detecting changes in the magnetic permeability within its core. The impedance of the coil has the general form:

$$Z_{coil} = R + jX. \quad (5)$$

Therefore, we can extract the reactance from the imaginary component of Eq. (3):

$$X_{coil} = \frac{\omega[L(1 - \omega^2 LC_{par}) - C_{par}R_{par}^2]}{(1 - \omega^2 LC_{par})^2 + (\omega C_{par}R_{par})^2}. \quad (6)$$

To measure the magnetic permeability or magnetization of a magnetic thin film, such as a 2D-TMD DMS, subjected to an external stimulus such as light, the magnetic film is positioned within the core of the coil, and the reactance of the coil is measured during light irradiation. According to Eq. (6), the reactance (X) of the coil is strongly dependent on the induction (L) through the coil's core. Since the film is ferromagnetic, it will alter the relative permeability of the space within the coil, thereby changing the magnetic flux through the coil and consequently the reactance of the coil. As the microwire itself is ferromagnetic, the magnetization of the film will also lead to a change in the effective permeability of the microwire. Thus, the reactance of the sensor depends on this effective permeability, $X = X(\mu_{eff})$. Changes in the permeability of the film upon light illumination (i.e., the presence of additional holes mediating the magnetism in 2D-TMDs) will influence the effective permeability of the coil, which can be accessed through the change in its reactance: $\Delta X = X(\mu_{eff}, laser\ on) - X(\mu_{eff}, laser\ off)$. This change in reactance (ΔX) is proportional to the change in magnetization ΔM of the film upon light illumination, as illustrated in [Fig. 3c-f](#) for the case of a V-doped WS₂ monolayer. Using the MLCR method, we investigate the optically tunable magnetic properties of selected 2D-TMD DMSs and their heterostructures, with some of the results presented and discussed below.

3. Light-Tunable Two-Dimensional Magnetism

3.1. Magnetically Doped Transition Metal Dichalcogenide Monolayers

Among 2D vdW materials, 2D-TMDs are a fertile ground for novel quantum phenomena including nontrivial electronic topology, non-saturating giant magnetoresistance, and topological field-effect transistors [1,3,4,7]. Recently, TMD monolayers (e.g., WS_2 , WSe_2 , MoS_2) doped with magnetic transition metal atoms (e.g., V, Fe, Co, Cr) have been reported to exhibit room-temperature ferromagnetic order, emerging as a novel class of 2D-DMSs [52-71]. We have discovered tunable room-temperature ferromagnetism in V- WS_2 and V- WSe_2 monolayers by varying the V-doping concentration [52,53]. Figure 4 highlights some notable features of these 2D magnets.

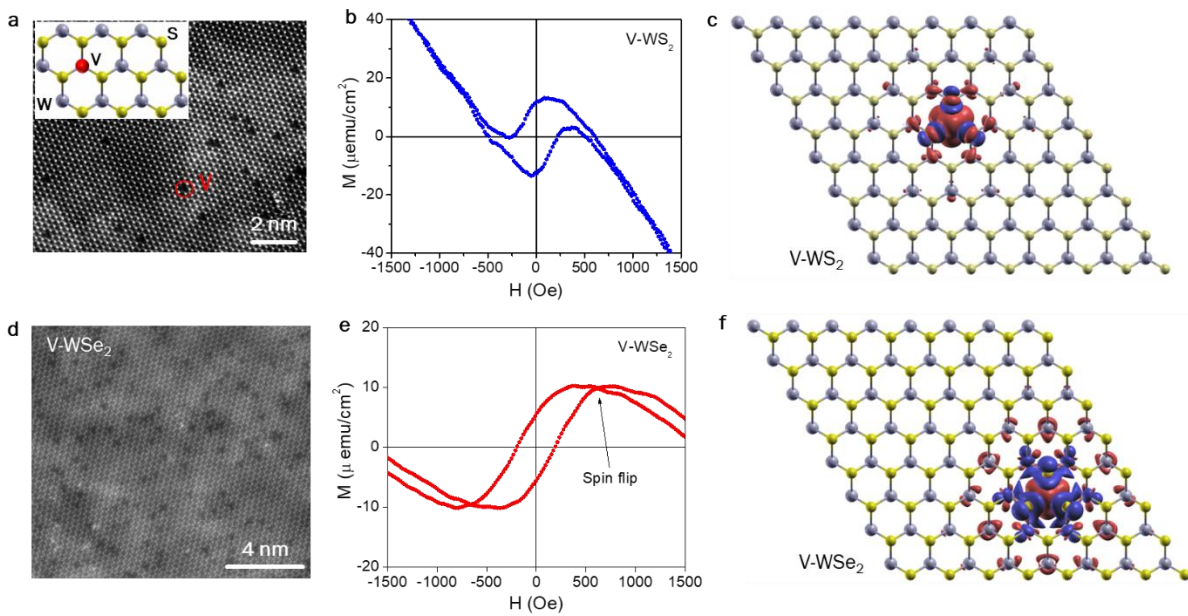


Figure 4. HRTEM images, magnetic hysteresis loops $M(H)$, and spin configurations of (a,b,c) 2 at.% V-doped WS_2 and (d,e,f) 4 at.% V-doped WSe_2 monolayers, respectively. Within the V- WS_2 monolayer, the magnetic moment of V (replacing one W) is *ferromagnetically* coupled to the magnetic moments induced at the nearest and further distance W sites (all red, see panel c). In the V- WSe_2 monolayer, the magnetic moment of V is *antiferromagnetically* coupled to the magnetic moments at the nearest distance W sites (blue vs. red, see panel f) but *ferromagnetically* coupled to

those at the further distance W sites (red, see panel **f**). It is the antiferromagnetic (AFM) coupling between the V and W spins at the nearest distance that leads to the thermally induced spin flipping phenomenon manifested as a crossover of magnetization in the $M(H)$ loop. Panels (a,b) are taken with permission from Ref. [52]; Panels (d,e) are taken with permission from Ref. [53].

By varying V-doping concentrations, we have demonstrated an enhanced magnetization and achieved the highest doping levels ever attained for atomically thin vanadium doped TMDs (~2 at.% for V-doped WS₂ monolayers [52], and ~4 at.% for V-doped WSe₂ monolayers [53]). Unlike the case of V-WS₂ monolayers (Fig. 4b,c), we have observed the thermally induced spin flipping (TISF) phenomenon in V-WSe₂ monolayers (Fig. 4e) due to the presence of antiferromagnetic coupling between spins at V-sites and their nearest W sites (Fig. 4f). Interestingly, the TISF phenomenon can be achieved at low magnetic fields (less than 100 mT) and manipulated by modifying the vanadium concentration within the WSe₂ monolayer. These 2D DMSs can thus be used as novel 2D spin filters to enhance the spin to charge conversion efficiency of spin-caloritronic devices [84,109]. It has been reported that after magnetic transition metal (e.g., V or Fe) doping, the photoluminescence signal is strongly suppressed in 2D-TMDs [52,53,55,61], which has been attributed to the formation of impurity energy bands caused by p-type doping at the valence band maximum [51-53,72]. Therefore, it is crucial to select appropriate doping concentrations at which 2D-TMDs exhibit optimized magnetic and optical properties.

Duong *et al.* studied the effect of electric gating on the magnetization of V-doped WSe₂ monolayers and found that hole injection enhances the magnetization, while electron injection significantly decreases it [54,57]. Complementing experimental findings, DFT calculations reveal the dominant hole-mediated long-range ferromagnetic interactions between V-spins in atomically thin V-doped TMD systems [57]. Our previous studies have shown that, after vanadium doping, significant photoluminescence is still present in 2 at.% V-doped WS₂ [52] and 4 at.% V-doped WSe₂ [53]

monolayers, which both exhibit the largest saturation magnetization (M_S) values among the compositions investigated. These observations have led us to propose that the ferromagnetism in the V-WS₂ or V-WSe₂ monolayer can be mediated by illumination with a laser of appropriate energy, specifically, above the optical gap (Fig. 3c). Electrons from photogenerated electron-hole pairs may be captured by the V atoms, thus creating an imbalance in the carrier population (i.e., the generation of excess holes) such that the ferromagnetism of the monolayer is modified (Fig. 3d-f).

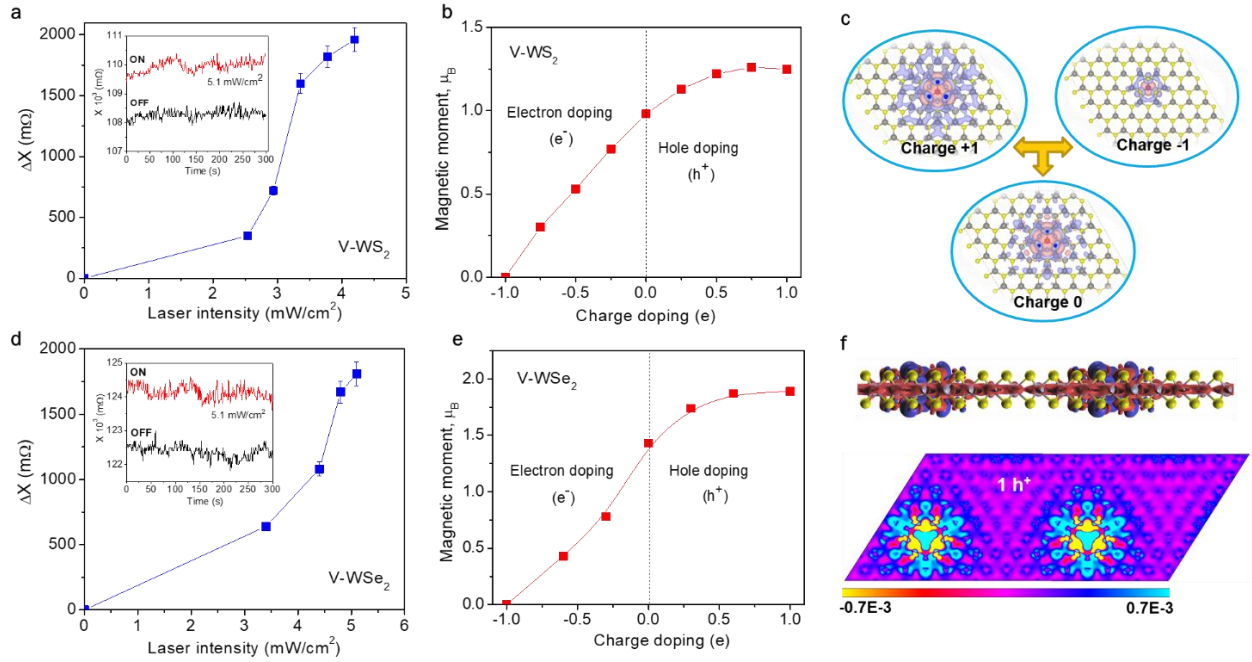


Figure 5. The laser intensity dependence of the change in reactance (ΔX) of (a) V-WS₂ and (d) V-WSe₂ monolayers. Insets show the change in reactance upon light illumination with a 650 nm laser for (a) V-WS₂ and (d) V-WSe₂ monolayers; The net magnetic moments of (b) V-WS₂ and (e) V-WSe₂ monolayers with different carrier doping densities; (c) The projected magnetic moment along the c-axis of the V-WS₂ monolayer upon one hole and one electron injection relative to no charge injection; (f) The projected magnetic moment along the c-axis of the V-WSe₂ monolayer upon a single hole injection. Hole injection increases the magnetization of the V-WS₂ or V-WSe₂ monolayer. Panels (a,b,c) taken with permission from Ref. [56]; Panel (f) taken with permission from Ref. [57].

The combination of magnetic and semiconducting properties in 2D-TMD DMSs has indeed enabled light modulation and tunability of magnetization, as demonstrated for V-WS₂ and V-WSe₂ monolayers (Fig. 5). As can be clearly seen from Fig. 5(a,d), both V-WS₂ and V-WSe₂ systems exhibit a similar light intensity-dependent magnetization trend. Note that undoped TMD samples (pristine WS₂ and WSe₂ monolayers) do not exhibit light-mediated magnetism, and the observed enhancement of the magnetization in illuminated V-doped TMD monolayers is not due to a laser/sample heating effect but originates from carrier-mediated ferromagnetism, similar to the case of a p-type (In,Mn)As/GaSb semiconductor [110]. DFT calculations demonstrate that hole injection shifts the Fermi level deeper inside the valence band, while electron injection shifts it towards the conduction band edge [56,57]. As a result, the magnetic moment becomes larger with increasing hole concentration, while an opposite trend is observed for electron injection (Fig. 5b,e). Increasing the concentration of holes results in a more robust magnetic moment across the lattice, where W atoms far from the V site exhibit an enhanced magnetic moment. Since long-range ferromagnetic interactions are mediated by free holes in V-WS₂ and V-WSe₂ systems it is unsurprising that optically injecting hole-carriers leads to enhanced ferromagnetism. The theoretical calculations fully support the experimental findings. It is worth noting that at large hole concentrations, the magnetic moment saturates, confirming the feature observed experimentally (Fig. 5a,d). This has been attributed to the screening of charge carriers at high hole concentrations. The experimental results presented in Fig. 5 were obtained from MLCR experiments conducted using a 650 nm laser. We also performed MLCR measurements on the same samples using a 520 nm laser and observed enhanced magnetization, confirming that light-enhanced magnetization can be achieved with any wavelength above the optical gap.

Although the V-WS₂ and V-WSe₂ systems share a similar light-mediated magnetization effect (Fig. 5a,d), a noticeable difference in magnetic coupling between spins at a V-site and its nearest W-sites (namely, the nearest V-W spins) is evident [56,57]. DFT calculations reveal that interactions between the nearest V-W spins are *ferromagnetic* in V-WS₂ monolayers [52,56] but *antiferromagnetic* in V-WSe₂ monolayers at the same V-doping level [53,57]. In the case of V-WS₂ monolayers, the ferromagnetic interaction between the nearest V-W spins becomes stronger with increasing hole concentration (or increase of light intensity), giving rise to an enhanced magnetic moment (Fig. 5c). However, the situation is rather different for V-WSe₂ monolayers (Fig. 5f), in which the V atom couples antiferromagnetically to the nearest W sites, and ferromagnetically to the distant W-sites. The introduction of charge carriers mediates this interaction, where increasing hole carriers results in an enhanced magnetic moment at the V site. Additionally, the magnetic moment at the near W sites, flips from antiferromagnetic to weakly ferromagnetic, which combined with the increasing magnetic moment at the V site, results in the enhanced long-range ferromagnetism (Fig. 5f). What is particularly striking in the V-WSe₂ system, is the antiferromagnetic coupling between V and near W sites, which appears to be responsible for the lack of saturation of the magnetic moment at higher laser intensities (Fig. 5d).

These findings suggest that the light-mediated magnetism effect is *universal* to the class of 2D-TMD DMS and should be fully exploited for applications in opto-spintronics, opto-spin-caloritronics, spin-valleytronics, and quantum communications.

3.2. Two-Dimensional Transition Metal Dichalcogenide Heterostructures

Typical vdW TMD monolayers offer extensive flexibility and integration with one another [7,8,15,17,51]. Stacking different 2D-TMDs can create novel heterostructures with atomically sharp interfaces and properties that would otherwise be absent in their individual components [15,17,51]. Recent studies have demonstrated that the magnetic or magneto-optical properties of a non-magnetic

TMD (e.g., WS₂, MoS₂) can be induced or enhanced by stacking it with another magnetic TMD (VS₂, VSe₂, CrSe₂, MnSe₂) [13,50,111-113]. This occurs as a result of combined charge transfer and magnetic proximity (PM) effects [13,50,80,113]. By forming MoS₂/VS₂ and WS₂/VS₂ interfaces, DFT calculations indicate that charge transfer occurs across the interface from MoS₂ or WS₂ to VS₂, as both MoS₂ and WS₂ have smaller work functions compared to VS₂ [113]. Electrons accumulate in the VS₂ layer, while holes occupy the MoS₂ or WS₂ layer. Consequently, both MoS₂/VS₂ and WS₂/VS₂ heterostructures exhibit enhanced magnetic properties, with Curie temperatures exceeding 300 K [113]. By forming CrSe₂/WSe₂ interfaces, DFT calculations by Li *et al.* also show that charge transfer from the WSe₂ to the CrSe₂ layer and interlayer coupling within CrSe₂ play crucial roles in the magnetic properties of the heterostructure [50]. A similar situation is anticipated in VSe₂/MoS₂ and MnSe₂/MoTe₂ systems [13,112], where both VSe₂ and MnSe₂ monolayers have been reported to display ferromagnetism above room temperature [13,14]. The combined semiconducting and ferromagnetic properties make these heterostructures appealing for opto-spintronics and opto-spin-caloritronics, as the application of external stimuli such as electric gating and light is likely to promote the charge transfer process and hence alter the magnetic and magneto-optic properties of the heterostructures [87].

As demonstrated above for V-WS₂ and V-WSe₂ monolayers, the magnetic and semiconducting properties coexist, giving rise to their magneto-optical properties and granting access to the rich electronic properties of 2D semiconductors, enabling the light tunability of magnetization. These findings suggest a similar phenomenon in VSe₂/WS₂ and VSe₂/MoS₂ heterostructures. An intriguing feature of the VSe₂/WS₂ or VSe₂/MoS₂ heterostructure is the presence of strong interfacial magnetic coupling and the potential for charge transfer between the two layers, which may play a key role in mediating the magnetization of the film. Bilayer MoS₂ shows a strong photon absorption peak around 600-700 nm, and by illuminating the VSe₂/MoS₂ film with energy close to the peak, we expect

considerable photogeneration of electron-hole pairs. These pairs may be separated through the electric field at the heterointerface, which leads to the observed light-tunable magnetism in the film.

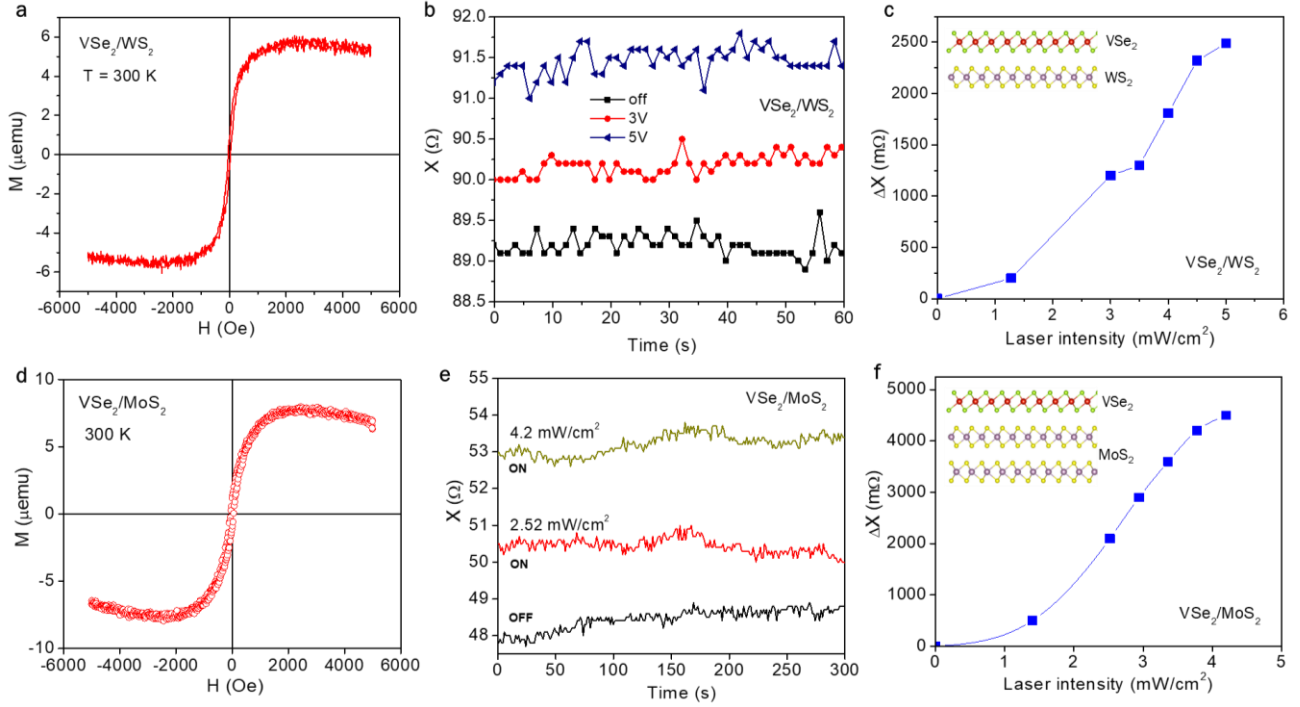


Figure 6. Magnetic hysteresis loops ($M(H)$) taken at 300 K for (a) 1L-VSe₂/1L-WS₂ and (d) 1L-VSe₂/2L-MoS₂ films. The reactance (X) vs. time upon illumination with a 650-nm laser with various intensities for (b) 1L-VSe₂/1L-WS₂ and (e) 1L-VSe₂/2L-MoS₂ films. Laser intensity dependence of the reactance change (ΔX) for (c) 1L-VSe₂/1L-WS₂ and (f) 1L-VSe₂/2L-MoS₂ films.

To investigate this hypothesis, we conducted MLCR experiments on both VSe₂/WS₂ and VSe₂/MoS₂ heterostructure samples upon light illumination using a diode laser with a wavelength of ~ 650 nm ($h\nu \sim 1.91$ eV). In this case, the VSe₂/WS₂ or VSe₂/MoS₂ heterostructure consists of a vertically stacked monolayer (1L) VSe₂ and monolayer (1L) WS₂ or bilayer (2L) MoS₂ grown on an SiO₂ substrate by combining molecular beam epitaxy (MBE) and chemical vapor deposition (CVD), respectively. Representative results of the VSe₂/WS₂ and VSe₂/MoS₂ samples are displayed in Fig. 6. It is noteworthy to observe that both the 1L-VSe₂/1L-WS₂ and 1L-VSe₂/2L-MoS₂ samples exhibit a pronounced ferromagnetic signal at room temperature (Fig. 6a,d), as well as light-tunable

ferromagnetism at room temperature (Fig. 6b,e). For both heterostructures, the magnetization significantly increases with increasing laser intensity and tends to saturate at high laser intensities (Fig. 6c,f). The light intensity dependence of magnetization for the VSe₂/WS₂ and VSe₂/MoS₂ heterostructures (Fig. 6c,f) is similar to that observed for V-doped TMD monolayers (Fig. 5a,d) and for a CH₃NH₃PbI₃/LSMO heterostructure [96]. The enhancement and tunability of light-mediated ferromagnetism in the 1L-VSe₂/2L-MoS₂ film were also independently confirmed by the pump-probe MOKE technique [90]. It is important to note that this light-mediated magnetism effect is not observed in the individual layers (WS₂, MoS₂, VSe₂); only when they are stacked together do we observe light-dependent magnetization. These results demonstrate the universality of the light-mediated magnetism effect and pave a new pathway for the design and fabrication of novel van der Waals heterostructures for use in 2D van der Waals spintronics, opto-spin-caloritronics, and opto-valleytronics.

Comparison of the light-mediated magnetization results of 1L-VSe₂/2L/MoS₂ and 1L-VSe₂/BSC MoS₂ (BSC: Bulk single crystal) samples has shown that the change in magnetization in 1L-VSe₂/2L-MoS₂ is approximately 4 times greater than that of 1L-VSe₂/BSC-MoS₂ (Fig. 7a) and this result is reproducible (inset of Fig. 7a). This observation leads us to believe that electron confinement effects on the 2L-MoS₂ might play a significant role in the mechanism behind light mediated magnetism in this heterostructure (Fig. 7b), as compared to the case of BSC MoS₂ (Fig. 7c).

To elucidate the mechanism of light-enhanced magnetism in the 1L-VSe₂/2L-MoS₂ system, we conducted first-principles defect calculations [114] based on the Heyd-Scuseria-Ernzerhof (HSE) hybrid functional (with the mixing parameter set to 0.15) [115] as implemented in VASP [116] and with the van de Waals correction [117] and finite-supercell size effects [118] included. The calculations suggest that this enhancement can be tentatively attributed to the presence of sulfur vacancies (V_S) in 2L-MoS₂ (Fig. 7d-f). V_S are found to be stable in their negative charge states (V_S^-)

within the range of Fermi-level values closer to the conduction-band minimum (CBM). Under n-type conditions, V_S^- represents the lowest-energy magnetic native point defect ($1\mu_B$ per V_S^-) (Fig. 7e). The magnetic interaction between the two V_S^- defects is weakly ferromagnetic. In the VSe_2/MoS_2 system, the presence of the Vse_2 layer with a larger work function of ~ 4.5 eV (compared to ~ 4.1 eV for the MoS_2 layer) results in an accumulation of electrons in the Vse_2 layer, creating a depleted region in the MoS_2 side of the hetero-interface and subsequent formation of a Schottky barrier. The mechanism for ferromagnetism in the Vse_2/MoS_2 system remains under debate; however, the accumulation of electrons in the Vse_2 layer could give rise to enhanced ferromagnetism in this layer and thus contribute to the change in net magnetization of the Vse_2/MoS_2 heterostructure when the material is not exposed to light. It should be noted that 1L- Vse_2 has a more dominant magnetic contribution to the net magnetization of the 1L- $Vse_2/2L-MoS_2$ film.

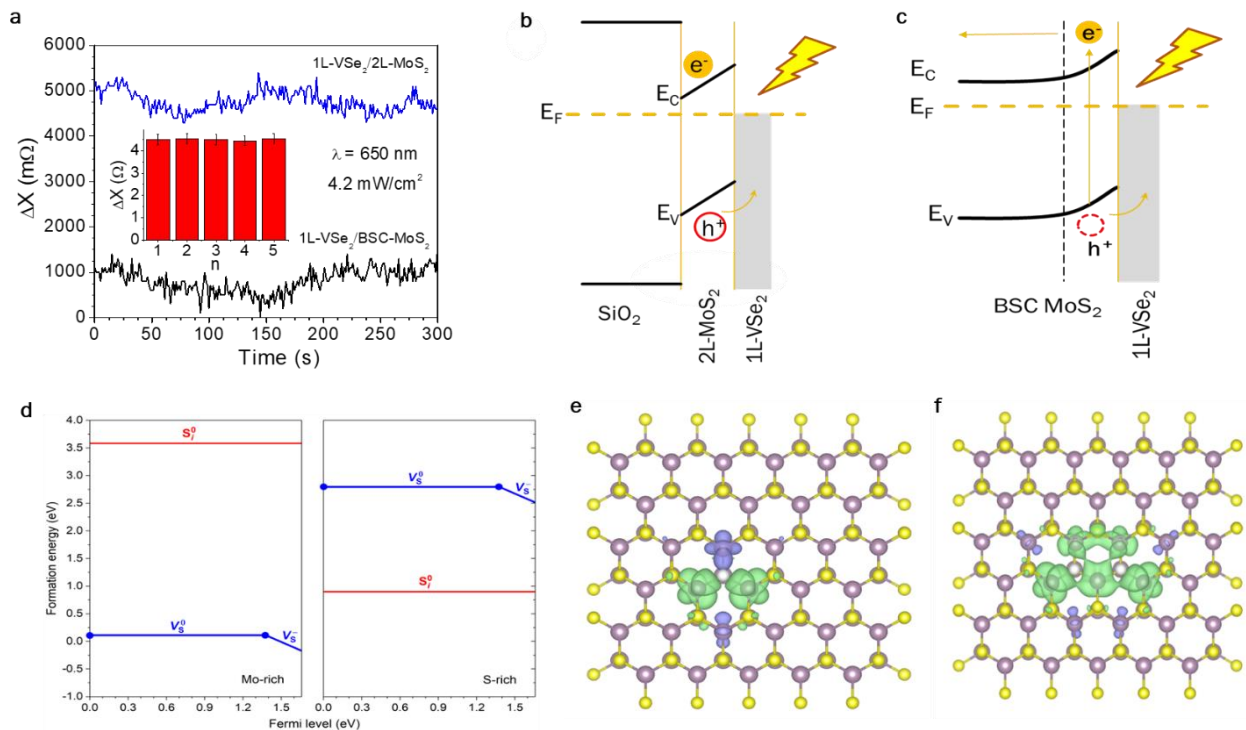


Figure 7. (a) Comparison of the reactance change (ΔX) due to light irradiation at the same wavelength ($\lambda = 650$ nm) and intensity (4.2 mW/cm 2) between the 1L- $Vse_2/2L-MoS_2$ film and the 1L- $Vse_2/BSC-$

MoS₂ film. Upon light irradiation, the enhancement of the magnetization is approximately 4 times greater in the 1L-Vse₂/2L-MoS₂ film than in the 1L-Vse₂/BSC-MoS₂ film. **Inset of (a)** shows values of the reactance change (ΔX) measured at different times demonstrating the reproducibility of the observed effect. Schematics show a possible charge transfer via **(b)** the 2L-MoS₂/Vse₂ and **(c)** BSC-MoS₂/Vse₂ interface upon light irradiation; **(d)** Formation energies of sulfur vacancies (V_S) and interstitials (S_i) in a 2H-MoS₂ bilayer under extreme Mo-rich and S-rich conditions and plotted as a function of the Fermi level from the VBM to the CBM. The slope of energy-line segments indicates the charge state. The vacancy (interstitial) is found to be the dominant native point defect under the Mo-rich (S-rich) condition. V_S is stable as the neutral (and nonmagnetic) vacancy V_S^0 in a wide range of Fermi-level values and as the negatively charged vacancy V_S^- near the CBM (i.e., under n-type conditions). The (0/-) transition level of V_S is at 0.31 eV below the CBM. V_S^- has a calculated magnetic moment of $1\mu_B$. S_i is, on the other hand, stable as the neutral and nonmagnetic vacancy S_i^0 in the entire range of Fermi-level values; **(e)** Top-view of spin density associated with a single negatively charged defect V_S^- ; **(f)** top-view of the spin density associated with a pair of V_S^- . Large (purple) spheres are Mo, and small (yellow) spheres are S. The lattice site of the vacancy is marked by a small (white) sphere. The isosurface level is set to $0.014 \text{ e}/\text{\AA}^3$ and the green (purple) isosurfaces correspond to up (down) spin.

Upon light illumination, electron-hole pairs are generated and subsequently separated by the interfacial electric field at the Schottky barrier between the two materials. Consequently, an accumulation of excited electrons builds up in the conduction band of MoS₂. This 2D electron gas can increase the negative charge of the sulfur vacancies in the MoS₂ layer, which, in turn, increases the net magnetic moment (**Fig. 7f**). For instance, the nonmagnetic V_S^0 becomes V_S^- , for a certain duration (during laser irradiation). Our calculations indicate that a portion of the extra electrons will

localize on the vacancy. At higher laser powers, more photo-generated electrons in the conduction band of MoS₂ will completely fill the available confined-states and eventually leak to the VSe₂ layer, which could explain the saturation of magnetization enhancement. Due to the two-dimensional nature of 2L-MoS₂, both photo-generated electrons and sulfur vacancies are confined to the vicinity of the heterostructure interface. This facilitates the ferromagnetic interaction between nearby neighboring vacancies, which not only leads to a larger magnetic moment in the film but also enhances light-controlled magnetism. This suggests that besides the interfacial coupling of the heterostructure, the electron confinement and the concentration of sulfur vacancies also mediate the change in magnetization of the film under illumination (see, Fig. 7a-c). This effect is significantly reduced when the thickness of the MoS₂ layer is increased, as demonstrated by the change in magnetization of the BSC-MoS₂/VSe₂ being 4 times smaller than that of 2L-MoS₂/VSe₂ (Fig. 7a). We attribute this to the lack of confinement near the MoS₂/VSe₂ interface. In the case of BSC-MoS₂/VSe₂ (Fig. 7c), photogenerated electrons are no longer confined to the interface but can move deeper into the MoS₂ layer, significantly reducing the concentration of electrons near the interface. Nevertheless, further studies are required to fully understand the mechanism of light-mediated ferromagnetism in the VSe₂/MoS₂ system. It should also be noted that sulfur vacancies in 2L-MoS₂ are likely not the sole source of magnetism; other point defects and extended defects in the samples may play a role. Our theoretical argument regarding light-enhanced ferromagnetism is applicable to any defect whose electrical and magnetic properties resemble those of sulfur vacancies.

4. Opportunities and Challenges

Our findings have established that the light-modulated magnetism effect is *universal* to 2D-TMD DMSs, including V-doped TMD monolayers (V-WS₂, V-WSe₂, and V-MoS₂). In addition to their electrically tunable magnetic functionalities, the optically tunable atomic-level magnetism at room temperature makes 2D-TMD DMSs even more attractive for applications in spintronics, spin-

caloritronics, and valleytronics. It is worth noting that both electrons and holes are populated in light-illuminated MLCR experiments, while the DFT simulations consider the separated effect for each type of carrier. The coexistence of magnetic and semiconducting properties is necessary; therefore, higher doping concentrations are unlikely to exhibit this effect, as their semiconducting qualities are strongly suppressed. On the other hand, lower V-doping concentrations are interesting to study, since excellent semiconducting properties are preserved while the magnetic moment is slightly smaller compared to optimally V-doped TMD samples. Investigating the influence of different V doping concentrations on 2D-TMDs' light-mediated magnetism effect is an intriguing direction for future research. Further studies are necessary to understand the relationship between doping concentration and light-enhanced magnetism.

In addition, we have demonstrated the universality of the light-mediated magnetism effect in 2D-TMD ferromagnet/semiconductor heterostructures, including VSe_2/WS_2 and VSe_2/MoS_2 systems. Charge transfer, proximity, and confinement effects play a crucial role in enhancing light-mediated magnetization in these 2D systems. However, other effects such as interdiffusion, intercalation, twisting, and moiré patterns, which could occur during heterostructure formation remain largely unexplored [31,45,51,78,99,119]. Recently, Wang *et al.* revealed the novel possibility of tuning spin-spin interactions between moiré-trapped holes using optical means, inducing a ferromagnetic order in WS_2/WSe_2 moiré superlattices [99]. In the case of VSe_2/MoS_2 heterostructures, the moiré pattern has been observed at low temperatures (below the charge density wave transition temperature, T_{CDW}), and the presence of this moiré pattern led to enhanced magnetization, strong interfacial magnetic coupling, and the exchange bias (EB) effect within this temperature range [13,85]. To fully understand the moiré effect, and to exploit the light tunability of the EB effect, it would be interesting to investigate the light-mediated magnetism effect in VSe_2/MoS_2 and VSe_2/WS_2 heterostructures at $T < T_{CDW}$. DFT calculations suggest that charge transfer from the ferromagnetic metal VSe_2 ($CrSe_2$) to

the semiconductor MoS₂ (WSe₂) gives rise to the magnetic moment of the MoS₂ (WSe₂) layer. A fundamental question emerges: *Will a similar effect occur when the 2D semiconducting TMD (MoS₂, WS₂, etc.) layer interfaces with a non-magnetic metal like graphene?* Exploring magnetism and light effects in semiconducting 2D-TMDs (both pristine and magnetically doped TMDs) interfaced with graphene will not only address this important question but also provide new insights into charge transfer-mediated magnetism in light-illuminated van der Waals heterostructures composed of 2D-TMD DMSs and other 2D materials. Depending on the work function difference between the two component materials, holes/electrons can be transferred into 2D-TMD DMSs, resulting in enhanced or reduced magnetization. This represents a promising, innovative approach for designing novel 2D-TMD heterostructures with enhanced magnetic and magneto-optic properties through a combined chemical doping and interface engineering (via the light-modulated directional charge transfer mechanism) strategy.

From an application perspective, the optically tunable magnetic properties of 2D-TMD DMSs and heterostructures are desirable for opto-spintronics, opto-spin-caloritronics, and valleytronics. Ghiasi *et al.* demonstrated charge-to-spin conversion across a monolayer WS₂/graphene interface due to the Rashba-Edelstein effect (REE) [120]. Alternatively, using 2D-TMD DMSs such as V-WS₂ and V-WSe₂ monolayers may not only boost spin-charge conversion efficiency but also enable optical manipulation of the spin-charge conversion process. A comprehensive review by Sierra *et al.* highlighted the novel application perspectives of opto-spintronics [7].

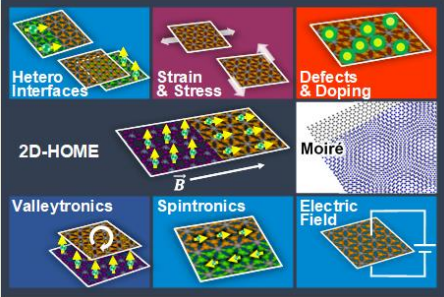
Thermally induced spin currents based on the spin Seebeck effect (SSE), a phenomenon discovered by Uchida *et al.* [121,122], laid the foundation for a new generation of spin-caloritronic devices. A pure spin current can be generated in a ferromagnetic (FM) material (like YIG: Y₃Fe₅O₁₂) due to a built-up electric potential across a temperature gradient upon the application of a magnetic field. This spin current can be converted into a technologically useful voltage via the inverse spin

Hall effect of a heavy metal (HM) with strong spin-orbit coupling (like Pt) in an FM/HM structure. Recently, Kalappattil *et al.* showed that inserting a thin (~5 nm) organic *semiconducting* layer of C₆₀ can significantly reduce the conductivity mismatch between YIG and Pt and the surface perpendicular magnetic anisotropy of YIG, resulting in a giant enhancement (600%) in the longitudinal SSE [91]. Following this approach, Lee *et al.* inserted a *semiconducting* WSe₂ monolayer between Pt and YIG and observed the giant SSE in Pt/WSe₂/YIG [123]. DFT calculations indicate that inserting a 2D-TMD DMS (e.g., V-WSe₂) in an FM/HM bilayer system not only reduces the conductivity mismatch but also enhances the spin mixing conductance and hence the spin-to-charge conversion efficiency via the SSE [123]. By taking advantage of the light-tunable magnetization of 2D-TMD DMSs [56,90], Phan *et al.* recently proposed a new route for the optical control of thermally induced spin currents through 2D-TMD DMS interfaces in FM/HM systems, establishing the new subfield named “Opto-spin-caloritronics” [84], which can harness “*light as the new heat*”. Further studies are needed to fully exploit this potential.

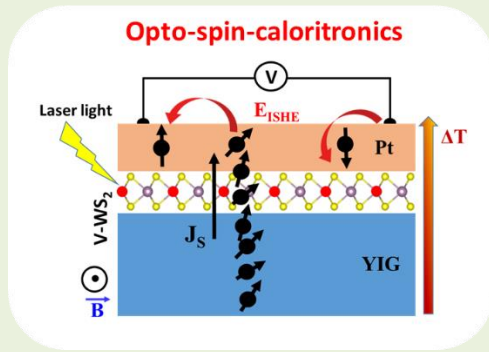
Semiconducting 2D-TMDs (e.g., WSe₂, WS₂, MoS₂) are excellent candidates for use in valleytronic devices [48,49]. Controlling and manipulating the valley polarization states in these 2D-TMDs using external stimuli (optic, electric, and magnetic field) is essential [77,124-127]. Doping magnetic atoms (Fe, V) into a MoS₂ monolayer to form Fe-MoS₂ [66] or V-MoS₂ [67] DMSs has been reported to enhance valley splitting in MoS₂ monolayers. Since 2D-TMD DMSs exhibit strong magnetic responses to both electric fields and lasers [56,57], their valleytronic properties can be manipulated by these external stimuli. Seyler *et al.* [41] experimentally exploited light to control CrI₃ magnetization in a CrI₃/WSe₂ heterostructure, demonstrating the optical modulation of valley polarization and valley Zeeman splitting within the WSe₂ monolayer. However, the CrI₃ monolayer exhibits ferromagnetic ordering below 50 K, rendering the CrI₃/WSe₂ heterostructure impractical for use in valleytronic devices that operate at ambient temperatures. In this context, the optical

modulation of magnetic and valleytronic properties of $\text{VSe}_2(\text{MnSe}_2)/\text{MoS}_2$ and $\text{VSe}_2(\text{MnSe}_2)/\text{WS}_2$ heterostructures appears more compelling, as the VSe_2 or MnSe_2 layer exhibits ferromagnetic order above room temperature [13,14]. Based on DFT calculations, He *et al.* showed that an ultrafast laser pulse can induce a ferromagnetic state in a nonmagnetic MoSe_2 monolayer when interfaced with the MnSe_2 monolayer, which orders ferromagnetically above room temperature [128]. Such ultrafast optical control of 2D magnetism is highly compelling for applications in ultrafast spintronics and magnetic storage information technology [129]. It is worth noting that the magnetic properties of 2D-TMDs have contributions from defect- and dopant-induced magnetic moments and their couplings [51,60]. Therefore, it would be of significant interest to investigate the effects of transition metal or chalcogen vacancies and magnetic dopant concentrations on the magnetic, magneto-optic, and valleytronic properties of free-standing TMD monolayers, as well as those placed on magnetic substrates in heterostructures. Scheme 1 highlights opportunities and challenges in exploiting 2D-TMD DMSs and heterostructures for use in modern nanodevices.

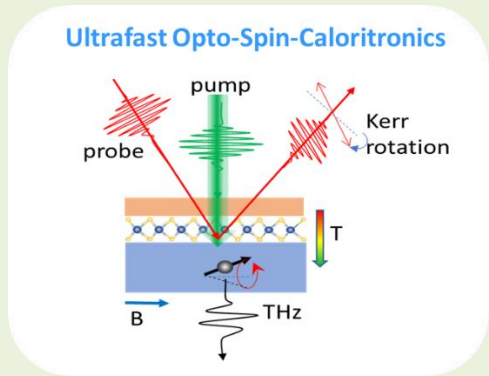
Scheme 1. Opportunities and challenges in the research of 2D-TMD magnets.

Two-dimensional van der Waals Dilute Magnetic Semiconductors	
Opportunities	Challenges
<ul style="list-style-type: none"> Electrically and optically tunable magnetism in 2D-TMD DMSs (e.g., V-doped WSe₂) for spin transistors, sensors, and spin-logic device applications  <ul style="list-style-type: none"> Optically tunable twisted and moiré magnetism and related phenomena in 2D-TMD heterostructures (e.g., VSe₂/MoS₂, WS₂/WSe₂) for spintronics and opto-spintronics Exploring light-tunable exchange bias or exchange anisotropy in 2D vdW heterostructures (e.g., VSe₂/MoS₂, VS₂/WS₂) for opto-spintronics Optically tunable magnetism and spin-thermo-transport (SSE, ANE, etc.) in 	<ul style="list-style-type: none"> Weak ferromagnetism Difficulty controlling magnetic dopants/defects in 2D-TMDs to achieve reproducible magnetic properties (e.g., M_s, H_c) Strong suppression of ferromagnetism and photoluminescence in heavily doped 2D-TMDs Air instability (magnetic signals are degradable when exposed to air) Difficulty with integration and fabrication of 2D-TMD-based devices Air instability (magnetic degradation causes the SSE voltage to reduce) Gaps in understanding spin-charge-phonon coupling mechanisms that govern spin transport across 2D vdW interfaces Large discrepancy between the theoretical and experimental values of SSE voltage for the reported 2D magnets and heterostructures

FM/2D-TMD/HM structures (e.g., YIG/ML V-doped WSe₂/Pt) for opto-spin-caloritronics



- Ultrafast magnetism and ultrafast spin-thermo-transport for ultrafast opto-spin-caloritronic device applications



- Need to select vdW materials that order magnetically at high temperatures (T_C , T_N) to achieve EB effects around room temperature
- Difficulty synthesizing and stacking vdW magnetic materials into heterostructures
- Surface and interface oxidization (magnetic degradation)
- Undesired effects of intercalation, interdiffusion at vdW magnet/metal interfaces, twisting, moiré patterns, etc.
- MOKE signals depend on quality of surfaces and interfaces of materials used; nonlocal heating effects on spin dynamics and transport
- Complex device structures and short lifetime of the devices

5. Concluding Remarks and Outlook

We have established the universality of the light-modulated magnetization effect in 2D-TMD DMSs, including V-doped TMD monolayers (V-WS₂, V-WSe₂, V-MoS₂). This effect is attributed to the presence of excess holes in the conduction and valence bands, as well as carriers trapped in the magnetic doping states, which mediate the magnetization of the TMD layer. Additionally, we have demonstrated the universality of the light-mediated magnetism effect in 2D-TMD ferromagnet/semiconductor heterostructures such as VSe₂/WS₂ and VSe₂/MoS₂. This effect is

attributed to photon absorption at the TMD layer (e.g., WS₂, WSe₂, MoS₂), generating electron-hole pairs that mediate the magnetization of the heterostructure. These findings pave a new pathway for the design of novel 2D-TMD van der Waals heterostructures that exhibit unique magneto-optical coupling functionalities that enable the next generation of high-performance optoelectronics, ultrafast opto-spintronics, opto-spin-caloritronics, valleytronics, and quantum technologies.

We have demonstrated the importance of proximity, charge-transfer, and confinement effects in enhancing light-mediated magnetization in 2D-TMD heterostructures, but other effects such as interdiffusion, intercalation, twisting, and moiré patterns may also be significant [31,45,51,78,99,119]. Further studies are thus needed to fully understand these effects. It appears that 2D-TMD magnetism arises from multiple contributions of vacancy- and dopant-induced magnetic moments, as well as their magnetic couplings, whose strengths vary depending on their complex vacancy-dopant configurations [51,60]. Understanding how light mediates magnetization in 2D-TMDs with controlled dopant/vacancy concentrations is critical. The “twisting” effect has been reported to significantly alter the magnetic and valleytronic properties of 2D-TMDs [130-135]. Twisting graphene from a 2D-TMD in a 2D-TMD/graphene heterostructure can enhance the valley Zeeman and Rashba effects [130,131], as well as the charge-to-spin conversion efficiency [132,133]. By tailoring the atomic interface between twisted bilayer graphene and WSe₂, Lin *et al.* showed strong electron correlation within the moiré flat band, which stabilizes insulating states at both quarter and half filling, and the spin-orbit coupling drives the Mott-like insulator into ferromagnetism [134]. In addition to the magnetic proximity and charge transfer effects, twisting adds an interesting experimental knob to tune the magnetic and magneto-optic functionalities of 2D-TMDs for spintronics and valleytronics applications.

From an application standpoint, the room-temperature electrically and optically tunable magnetic properties make 2D-TMD DMSs excellent candidates for use in spin transistors, logic, and

magnetic memory devices [51,54,86]. In opto-spintronics, ultrafast optical control of 2D magnetization may yield the fastest information recording and processing with minimal dissipative power [7,129]. Experimental studies are needed to verify these theoretical predictions [73,113]. Additionally, 2D-TMD DMSs can serve as novel 2D spin filters to boost the spin-to-charge conversion efficiency via the SSE in FM/2D-DMS/HM systems [84,109]. A comprehensive understanding of the spin-charge-phonon coupling mechanisms in such 2D spin filters is currently lacking but crucial for unlocking the potential of “Opto-Spin-Caloritronics,” which warrants further study.

Compared to their 2D-TMD counterparts, 2D-TMD DMSs appear more promising for use in valleytronic devices [66,67]. To further enhance the valley splitting in these 2D DMSs, it is possible to interface them with other 2D materials such as graphene. Combining chemical doping and interface engineering (charge transfer and/or strain) approaches can create 2D-TMD DMS/graphene or 2D-TMD DMS/2D-TMD heterostructures with enhanced magnetic, magneto-optic, and valleytronic properties that can be tuned by external stimuli (electric gating, light, strain). All these exciting possibilities will facilitate further research.

To provide insightful guidance on the development of 2D-TMD-based devices, we present in [Table 1](#) a list of promising 2D-TMD magnets and heterostructures. While most of the 2D-TMD DMSs are synthesized using chemical vapor deposition (CVD), some of their heterostructures are grown by molecular beam epitaxy (MBE) or a combination of both techniques [76]. CVD typically produces 2D films with uniformity, low porosity, high purity, and stability, but generates toxic gases during the reaction. MBE enables in-situ preparation of atomically clean substrates with specific surface reconstructions, facilitating the growth of highly epitaxial 2D films, but it can result in more defects during film growth [74-76]. It is essential to advance these techniques for growing defect-free or defect-controllable 2D-TMD DMSs and heterostructures.

As noted earlier, the high concentrations of magnetic dopants or the presence of abundant defects (transition metal/chalcogen vacancies) in 2D-TMD semiconductors lead to the strong suppression of photoluminescence [51-53]. However, co-doping with different metals such as, Co and Cr, in a MoS₂ monolayer has been reported to enhance both photoluminescence intensity and saturation magnetization [71]. Combining chemical co-doping and interface engineering represents a promising strategy for the design of 2D-TMD DMSs with enhanced magnetic and magneto-optic properties for spintronics, opto-spintronics, opto-spin-caloritronics, valleytronics, and quantum communications.

Acknowledgements

Research at USF was supported by the U.S. Department of Energy, Office of Basic Energy Sciences, Division of Materials Sciences and Engineering under Award No. DE-FG02-07ER46438 and the VISCOSTONE USA under Award No. 1253113200. M.T. acknowledges support from the Air Force Office of Scientific Research (AFOSR) through grant No. FA9550-18-1-0072 and the NSF-IUCRC Center for Atomically Thin Multifunctional Coatings (ATOMIC). This work used computing resources of the Center for Computationally Assisted Science and Technology (CCAST) at North Dakota State University, which were made possible in part by National Science Foundation Major Research Instrumentation (MRI) Award No. 2019077. The authors acknowledge Dr. M. Bonilla and Dr. S. Kolekar for assisting with the synthesis of VSe₂/MoS₂ samples.

Table 1. 2D-TMD magnets and heterostructures with optically tunable magnetic functionalities for spintronics, spin-caloritronics, and valleytronics.

Materials	Ordering temperature T_C (K)	Remarks	Ref.
Metals			
VSe ₂ (1L, 2L)	~270 – 350 K	Strong magnetism; Sensitive to defects; Less air stability	[13]
MnSe ₂ (1L, 2L)	~266 – 350 K	Intrinsic magnetism; Less sensitive to defects; Less air stability	[14]
CrSe ₂ (1L)	50~300 K	Intrinsic magnetism; Less sensitive to defects; Air stability	[50,136]
FeSe ₂ (1L)	~300 K	Intrinsic magnetism; Air stability	[136]
Semiconductors			
V-WS ₂ (1L) optimal ~2 at.%	~300 – 400 K	Unexplored optical control of valleytronic states; Less sensitive to air.	[52]
V-WSe ₂ (1L) optimal ~4 at.%	~300 – 400 K	Unexplored optical control of valleytronic states; Less sensitive to air.	[53]

V-MoSe ₂ (1L) optimal ~2 at.%	~300 – 400 K	Unexplored optical control of magnetism and valleytronic states; Less sensitive to air.	[63]
V-MoS ₂ (1L)	~300 – 400 K	Unexplored optical control of magnetism and valleytronic states; Less sensitive to air.	[61,67]
V-MoTe ₂ (1L)	~300 – 400 K	Unexplored optical control of magnetism and valleytronic states; Less sensitive to air.	[70]
Fe-MoS ₂ (1L)	~300 – 400 K	Unexplored optical control of magnetism and valleytronic states; Less sensitive to air.	[55,66]
Co-MoS ₂ (1L)	~300 K	Unexplored optical control of magnetism and valleytronic states; Less sensitive to air.	[58]
(Co,Cr)-MoS ₂ (1L)	~300 K	Unexplored optical control of magnetism and valleytronic states; Air stability.	[71]
Co-SnS ₂ (SC)	~120 K	Unexplored optical control of magnetism and valleytronic states; Air stability.	[138]

Fe-SnS ₂ (1L)	~30 K	Unexplored optical control of magnetism and valleytronic states; Air stability.	[139]
Mn-SnS ₂ (SC)	~150 K	Unexplored optical control of magnetism and valleytronic states; Air stability.	[140]
Heterostructures			
CrSe ₂ /WSe ₂ (1L/1L)	~50 – 120 K	Unexplored optical control of magnetism and valleytronic states; Charge transfer; Less sensitive to air.	[50]
VSe ₂ /MoTe ₂ (1L/1L)	~300 – 350 K	Unexplored optical control of magnetism and valleytronic states; Charge transfer; Less sensitive to air.	[111]
VSe ₂ /MoS ₂ (1L/2L)	~300 – 350 K	Unexplored optical control of valleytronic states; Observed EB effect; Charge transfer; Less sensitive to air.	[13,85]
MnSe ₂ /MoSe ₂ (1L/1L)	~300 – 350 K	Unexplored optical control of magnetism and valleytronic states; Charge transfer; Less sensitive to air.	[112]

VS ₂ /MoS ₂ (1L/1L)	~300 – 350 K	Unexplored optical control of magnetism and valleytronic states; Charge transfer; Less sensitive to air.	[137]
---	--------------	--	-------

References

1. P. Chuang, S.C. Ho, L.W. Smith, F. Sfigakis, M. Pepper, C.H. Chen, J.C. Fan, J.P. Griffiths, I. Farrer, H. E. Beere, G. A. C. Jones, D. A. Ritchie, and T.-M. Chen, All-electric all-semiconductor spin field-effect transistors, *Nat. Nanotech.* 10, 35 (2015).
2. F. Matsukura, Y. Tokura, H. Ohno, Control of magnetism by electric fields, *Nature Nanotechnology* 10, 209–220 (2015).
3. W.J. Yan, O. Txoperena, R. Llopis, H. Dery, L.E. Hueso & F. Casanova, A two-dimensional spin field-effect switch, *Nature Communications* 7, 13372 (2016).
4. B. Dieny et al., Opportunities and challenges for spintronics in the microelectronics industry, *Nature Electronics* 3, 446 (2020).
5. G. Faroz Ahmad Malik, M. Ahmad Kharadi, F. Ahmad Khanday, and N. Parveen, Spin field effect transistors and their applications: A survey, *Microelectronics Journal* 106, 104924 (2020)
6. J. Inгла-Aynés, F. Herling, J. Fabian, L.E. Hueso, and F. Casanova, Electrical Control of Valley-Zeeman Spin-Orbit-Coupling–Induced Spin Precession at Room Temperature, *Phys. Rev. Lett.* 127, 047202 (2021).
7. J.F. Sierra, J. Fabian, R.K. Kawakami, S. Roche, S.O. Valenzuela, Van der Waals heterostructures for spintronics and opto-spintronics, *Nat. Nanotechnol.* 16, 856–868 (2021).
8. A. Avsar, et al., Spintronics in graphene and other two-dimensional materials, *Rev. Mod. Phys.* 92, 021003 (2020).
9. E.C. Ahn, 2D materials for spintronic devices, *Npj 2D Mater. Appl.* 4, 1–14 (2020).
10. B. Huang, G. Clark, E. Navarro-Moratalla, D.R. Klein, R. Cheng, K.L. Seyler, D. Zhong, E. Schmidgall, M.A. McGuire, D.H. Cobden, others, Layer-dependent ferromagnetism in a van der Waals crystal down to the monolayer limit, *Nature.* 546, 270 (2017).

11. C. Gong, L. Li, Z. Li, H. Ji, A. Stern, Y. Xia, T. Cao, W. Bao, C. Wang, Y. Wang, others, Discovery of intrinsic ferromagnetism in two-dimensional van der Waals crystals, *Nature*. 546, 265 (2017).
12. Z. Fei, B. Huang, P. Malinowski, W. Wang, T. Song, J. Sanchez, W. Yao, D. Xiao, X. Zhu, A.F. May, others, Two-dimensional itinerant ferromagnetism in atomically thin Fe_3GeTe_2 , *Nat. Mater.* 17, 778 (2018).
13. M. Bonilla, S. Kolekar, Y. Ma, H.C. Diaz, V. Kalappattil, R. Das, T. Eggers, H.R. Gutierrez, M.H. Phan, M. Batzill, Strong room-temperature ferromagnetism in VSe_2 monolayers on van der Waals substrates, *Nat. Nanotechnol.* 13, 289 (2018).
14. D.J. O'Hara, T. Zhu, A.H. Trout, A.S. Ahmed, Y.K. Luo, C.H. Lee, M.R. Brenner, S. Rajan, J.A. Gupta, D.W. McComb, others, Room temperature intrinsic ferromagnetism in epitaxial manganese selenide films in the monolayer limit, *Nano Lett.* 18, 3125 (2018).
15. W. Li, Y. Zeng, Z. Zhao, B. Zhang, J. Xu, X. Huang, Y. Hou, 2D Magnetic Heterostructures and Their Interface Modulated Magnetism, *ACS Appl. Mater. & Interfaces*. 13, 50591 (2021).
16. G. Hu, B. Xiang, Recent Advances in Two-Dimensional Spintronics, *Nanoscale Res. Lett.* 15, 1–17 (2020).
17. T. Vincent, et al., Opportunities in electrically tunable 2D materials beyond graphene: Recent progress and future outlook, *Applied Physics Reviews* 8, 041320 (2021).
18. Y. Li, B.S. Yang, S.N. Xu, B. Huang, and W.H. Duan, Emergent Phenomena in Magnetic Two-Dimensional Materials and van der Waals Heterostructures, *ACS Appl. Electron. Mater.* 4, 3278 (2022).
19. H. Kurebayashi, J.H. Garcia, S. Khan, J. Sinova, S. Roche, Magnetism, symmetry and spin transport in van der Waals layered systems, *Nature Rev. Phys.* 4, 150 (2022).

20. M. Gibertini, M. Koperski, A.F. Morpurgo, K.S. Novoselov, Magnetic 2D materials and heterostructures, *Nat. Nanotechnol.* 14, 408 (2019).
21. Y. Khan, Sk. Md. Obaidulla, M.R. Habib et al., Recent breakthroughs in two-dimensional van der Waals magnetic materials and emerging applications, *Nano Today* 34, 100902 (2020).
22. X. Jiang, Q.X. Liu, J.P. Xing, N. Liu, Y. Guo, Z.F. Liu, and J. Zhao, Recent progress on 2D magnets: Fundamental mechanism, structural design and modification, *Appl. Phys. Rev.* 8, 031305 (2021).
23. S.Q. Zhang, R.Z. Xu, N. Luoc and X.L. Zou, Two-dimensional magnetic materials: structures, properties and external controls, *Nanoscale* 13, 1398 (2021).
24. W. Tang, H. Liu, Z. Li, A. Pan, Y.-J. Zeng, Spin-Orbit Torque in Van der Waals-Layered Materials and Heterostructures, *Adv. Sci.* 8, 2100847 (2021).
25. Y. Liu, Q. Shao, Two-dimensional materials for energy-efficient spin-orbit torque devices, *ACS Nano.* 14, 9389–9407 (2020).
26. J.F. Dayen, et al., Two-dimensional van der Waals spinterfaces and magnetic-interfaces, *Applied Physics Reviews* 7, 011303 (2020).
27. M.H. Phan, V. Kalappattil, V. Ortiz Jimenez, Y.T.H. Pham, N.W.Y.A.Y. Mudiyansele, D. Detellem, C.M. Hung, A. Chanda, and T. Eggers, Exchange Bias and Interface-related Effects in Two-dimensional van der Waals Magnetic Heterostructures: Open Questions and Perspectives, *Journal of Alloys and Compounds* 937, 168375 (2023).
28. C. Lei, et al., Magnetoelectric Response of Antiferromagnetic CrI₃ Bilayers, *Nano Lett.* 21, 1948 (2021).
29. S.W. Jiang, J. Shan, K.F. Mak, Electric-field switching of two-dimensional van der Waals magnets, *Nature Materials* 17, 406 (2018).

30. B. Huang, et al., Electrical control of 2D magnetism in bilayer CrI₃, *Nature Nanotechnology* 13, 544 (2018).
31. Y. Xu, et al., Coexisting ferromagnetic–antiferromagnetic state in twisted bilayer CrI₃, *Nature Nanotech.* 17, 143 (2022).
32. I. A. Verzhbitskiy, H. Kurebayashi, H. Cheng et al., Controlling the magnetic anisotropy in Cr₂Ge₂Te₆ by electrostatic gating, *Nat. Electron.* 3, 460 (2020).
33. W.H. Zhuo, et al., Manipulating Ferromagnetism in Few-Layered Cr₂Ge₂Te₆, *Adv. Mater.* 33, 2008586 (2021).
34. Z. Wang, et al., Electric-field control of magnetism in a few-layered van der Waals ferromagnetic semiconductor, *Nature Nanotechnology* 13, 554 (2018).
35. V. Ostwal, Efficient Spin-Orbit Torque Switching of the Semiconducting Van Der Waals Ferromagnet Cr₂Ge₂Te₆, *Adv. Mater.* 32, 1906021 (2020).
36. A. Ilyas, et al., Nonvolatile electrical control of 2D Cr₂Ge₂Te₆ and intrinsic half metallicity in multiferroic hetero-structures, *Nanoscale* 13, 1069 (2021).
37. V. Gupta, T.M. Cham, G.M. Stiehl, A. Bose, J.A. Mittelstaedt, K. Kang, S. Jiang, K.F. Mak, J. Shan, R.A. Buhrman, others, Manipulation of the van der Waals Magnet Cr₂Ge₂Te₆ by Spin-Orbit Torques, *Nano Lett.* 20, 7482 (2020).
38. Y.Y. Wu, et al., A Van der Waals Interface Hosting Two Groups of Magnetic Skyrmions, *Advanced Materials* 34, 2110583 (2022).
39. P. Zhang et al., All-optical switching of magnetization in atomically thin CrI₃, *Nat Mater.* 21, 1373-1378 (2022).
40. T.Y. Zhang et al., Laser-induced magnetization dynamics in a van der Waals ferromagnetic Cr₂Ge₂Te₆ nanoflake, *Appl. Phys. Lett.* 116, 223103 (2020).

41. Seyler, K. L. et al. Valley Manipulation by Optically Tuning the Magnetic Proximity Effect in $\text{WSe}_2/\text{CrI}_3$ Heterostructures. *Nano Letters* 18, 3823–3828 (2018).
42. R. Zhu, W. Zhang, W. Shen, P.K.J. Wong, Q. Wang, Q. Liang, Z. Tian, Y. Zhai, C. Qiu, A.T.S. Wee, Exchange Bias in van der Waals $\text{CrCl}_3/\text{Fe}_3\text{GeTe}_2$ Heterostructures, *Nano Lett.* 20, 5030 (2020).
43. M. Dąbrowski, Shi Guo, Mara Strungaru, Paul S. Keatley, Freddie Withers, Elton J. G. Santos, Robert J. Hicken. All-optical control of spin in a 2D van der Waals magnet. *Nature Communications* 13 (2022).
44. Z. Zhang, X.J. Ni, H.Q. Huang, L. Hu, and F. Liu, Valley splitting in the van der Waals heterostructure $\text{WSe}_2/\text{CrI}_3$: The role of atom superposition, *Phys. Rev. B* 99, 115441 (2019).
45. M. Ge, Han Wang, Jizheng Wu, Chen Si, Junfeng Zhang, and Shengbai Zhang, Enhanced valley splitting of WSe_2 in twisted van der Waals $\text{WSe}_2/\text{CrI}_3$ heterostructures, *npj Comput Mater* 8, 32 (2022).
46. T. Zhang, A. Wang, S. Li, F. Wang, Electrically and Magnetically Tunable Valley Polarization in Monolayer MoSe_2 Proximitized by a 2D Ferromagnetic Semiconductor, *Adv. Funct. Mater.* 32, 2204779 (2022).
47. B. Marfoua and J. Hong, Electric field dependent valley polarization in 2D $\text{WSe}_2/\text{CrGeTe}_3$ heterostructure, *Nanotechnology* 31, 425702 (2020).
48. S.A. Vitale, et al., Valleytronics: Opportunities, Challenges, and Paths Forward, *Small* 14, 1801483 (2018).
49. K.F. Mak, D. Xiao, and J. Shan, Light–valley interactions in 2D semiconductors, *Nature Photonics* 12, 451 (2018).
50. B. Li, et al., Van der Waals epitaxial growth of air-stable CrSe_2 nanosheets with thickness-tunable magnetic order, *Nature Materials* 20, 818 (2021).

51. Y.L. Huang, W. Chen, A.T.S. Wee, Two-dimensional magnetic transition metal chalcogenides, *SmartMat.* (2021).
52. F. Zhang, B. Zheng, A. Sebastian, D.H. Olson, M. Liu, K. Fujisawa, Y.T.H. Pham, V.O. Jimenez, V. Kalappattil, L. Miao, others, Monolayer vanadium-doped tungsten disulfide: a room-temperature dilute magnetic semiconductor, *Adv. Sci.* 7, 2001174 (2020).
53. Y.T.H. Pham, M. Liu, V.O. Jimenez, Z. Yu, V. Kalappattil, F. Zhang, K. Wang, T. Williams, M. Terrones, M.-H. Phan, Tunable ferromagnetism and thermally induced spin flip in Vanadium-doped tungsten diselenide monolayers at room temperature, *Adv. Mater.* 32, 2003607 (2020).
54. S.J. Yun, D.L. Duong, D.M. Ha, K. Singh, T.L. Phan, W. Choi, Y.-M. Kim, Y.H. Lee, Ferromagnetic order at room temperature in monolayer WSe₂ semiconductor via vanadium dopant, *Adv. Sci.* 7, 1903076 (2020).
55. S. Fu, K. Kang, K. Shayan, A. Yoshimura, S. Dadras, X. Wang, L. Zhang, S. Chen, N. Liu, A. Jindal, others, Enabling room temperature ferromagnetism in monolayer MoS₂ via in situ iron-doping, *Nat. Commun.* 11, 1–8 (2020).
56. V. Ortiz Jimenez, Y.T.H. Pham, M. Liu, F. Zhang, Z. Yu, V. Kalappattil, B. Muchharla, T. Eggers, D.L. Duong, M. Terrones, others, Light-Controlled Room Temperature Ferromagnetism in Vanadium-Doped Tungsten Disulfide Semiconducting Monolayers, *Adv. Electron. Mater.* 7, 2100030 (2021).
57. D.L. Duong, S.G. Kim, Y.H. Lee, Gate modulation of the long-range magnetic order in a vanadium-doped WSe₂ semiconductor, *AIP Advances* 10, 065220 (2020).
58. M. Huang et al., Direct Evidence of Spin Transfer Torque on Two-Dimensional Cobalt-Doped MoS₂ Ferromagnetic Material, *ACS Appl. Electron. Mater.* 2, 1497 (2020).

59. L.A.T. Nguyen et al., Spin-Selective Hole–Exciton Coupling in a V-Doped WSe₂ Ferromagnetic Semiconductor at Room Temperature, *ACS Nano* 15, 20267 (2021)
60. S.J. Yun et al., Escalating Ferromagnetic Order via Se-Vacancies Near Vanadium in WSe₂ Monolayers, *Advanced Materials* 34, 2106551 (2022).
61. J.Y. Seo, Controllable substitutional vanadium doping in wafer-scale molybdenum disulfide films, *Nano Research* 16, 3415 (2023).
62. S. Stolz et al., Layer-dependent Schottky contact at van der Waals interfaces: V-doped WSe₂ on graphene, *npj 2D Materials and Applications* 6, 66 (2022).
63. J. Deng et al., Vanadium-Doped Molybdenum Diselenide Atomic Layers with Room-Temperature Ferromagnetism, *Chem Phys Chem* 23, e202200162 (2022).
64. J. Zhang, et al., Vanadium-Doped Monolayer MoS₂ with Tunable Optical Properties for Field-Effect Transistors, *ACS Appl. Nano Mater.* 4, 769 (2021).
65. D.Y. Shen et al., Synthesis of Group VIII Magnetic Transition-Metal-Doped Monolayer MoSe₂, *ACS Nano* 16, 10623 (2022).
66. Q. Li, X. Zhao, L. Deng, Z. Shi, S. Liu, Q. Wei, L. Zhang, Y. Cheng, L. Zhang, H. Lu, others, Enhanced valley Zeeman splitting in Fe-doped monolayer MoS₂, *ACS Nano*. 14, 4636 (2020).
67. K.R. Sahoo, J.J. Panda, Sumit Bawari, Rahul Sharma, Dipak Maity, Ashique Lal, Raul Arenal, G. Rajalaksmi, and Tharangattu N. Narayanan, Enhanced room-temperature spin-valley coupling in V-doped MoS₂, *Phys. Rev. Materials* 6, 085202 (2022).
68. H.B. Shu, P.F. Luo, P. Liang, D. Cao, and X.S. Chen, Layer-Dependent Dopant Stability and Magnetic Exchange Coupling of Iron-Doped MoS₂ Nanosheets, *ACS Appl. Mater. Interfaces* 7, 7534 (2015).
69. B. Li et al., A two-dimensional Fe-doped SnS₂ magnetic semiconductor. *Nat. Commun.* 8, 1–7 (2017).

70. P.M. Coelho, H.-P. Komsa, K. Lasek, V. Kalappattil, Jeyakumar Karthikeyan, M.H. Phan, A. V Krasheninnikov, and M. Batzill, Room temperature ferromagnetic MoTe₂ by post-growth incorporation of vanadium impurities, *Advanced Electronic Materials* 5, 1900044 (2019).
71. H.L. Duan et al., Beating the exclusion rule against the coexistence of robust luminescence and ferromagnetism in chalcogenide monolayers, *Nature Communications* 10, 1584 (2019).
72. L. Cai, V. Tung, A. Wee, Room-temperature ferromagnetism in two-dimensional transition metal chalcogenides: Strategies and origin, *Journal of Alloys and Compounds* 913, 165289 (2022).
73. Y. Xiong, D. Xu, Y. Feng, G. Zhang, P-Type 2D Semiconductors for Future Electronics, *Adv. Mater.* , 2206939 (2023).
74. L. Loh, Z.P. Zhang, M. Bosman & G. Eda, Substitutional doping in 2D transition metal dichalcogenides, *Nano Research* 14, 1668 (2021).
75. Z.J. Zhao et al., Structure Engineering of 2D Materials toward Magnetism Modulation, *Small Structures* 2, 2100077 (2021).
76. Y.C. Lin et al., Controllable Thin-Film Approaches for Doping and Alloying Transition Metal Dichalcogenides Monolayers, *Advanced Science* 8, 2004249 (2021).
77. J.X. Li, et al., Electric control of valley polarization in monolayer WSe₂ using a van der Waals magnet, *Nature Nanotech.* 17, 721 (2022).
78. K. Zollner, Paulo E. Faria Junior, and Jaroslav Fabian, Proximity exchange effects in MoSe₂ and WSe₂ heterostructures with CrI₃: Twist angle, layer, and gate dependence, *Phys. Rev. B* 100, 085128 (2019).
79. B. Marfoua and J. Hong, Electric field dependent valley polarization in 2D WSe₂/CrGeTe₃ heterostructure, *Nanotechnology* 31, 425702 (2020).

80. C. Zhao, T. Norden, P. Zhang, P. Zhao, Y. Cheng, F. Sun, J. P. Parry, P. Taheri, J. Wang, Y. Yang, T. Scrace, K. Kang, S. Yang, G.-X. Miao, R. Sabirianov, G. Kioseoglou, W. Huang, A. Petrou, H. Zeng, Enhanced valley splitting in monolayer WSe₂ due to magnetic exchange field, *Nat. Nano.* 12, 757 (2017).
81. I. Khan, J. Ahmad, M.E. Mazhar, and J. Hong, Strain tuning of the Curie temperature and valley polarization in two dimensional ferromagnetic WSe₂/CrSnSe₃ heterostructure, *Nanotechnology* 32, 375708 (2021).
82. C.M. Hung, D.T.X. Dang, A. Chanda, D. Detellem, N. Alzahrani, N. Kapuruge, Yen T. H. Pham, M.Z. Liu, D. Zhou, H.R. Gutierrez, D.A. Arena, M. Terrones, S. Witanachchi, L.M. Woods, H. Srikanth, and M.H. Phan, Enhanced Magnetism and Anomalous Hall Transport through Two-dimensional Tungsten Disulfide Interfaces, *Nanomaterials* 13, 771 (2023).
83. J.W. Chu, Y. Wang, X. Wang, K. Hu, G.F. Rao, C.H. Gong, C.C. Wu, H. Hong, X.F. Wang, K.H. Liu, C.L. Gao, and J. Xiong, 2D Polarized Materials: Ferromagnetic, Ferrovalley, Ferroelectric Materials, and Related Heterostructures, *Adv. Mater.* 33, 2004469 (2021).
84. M.H. Phan, M.T. Trinh, T. Eggers, V. Kalappattil, K. Uchida, L.M. Woods, M. Terrones, A perspective on two-dimensional van der Waals opto-spin-caloritronics, *Appl. Phys. Lett.* 119, 250501 (2021).
85. M.H. Phan, V. Kalappattil, V. Ortiz Jimenez, Y.T.H. Pham, N.W.Y.A.Y. Mudiyansele, D. Detellem, C.M. Hung, A. Chanda, and T. Eggers, Exchange Bias and Interface-related Effects in Two-dimensional van der Waals Magnetic Heterostructures: Open Questions and Perspectives, *Journal of Alloys and Compounds* 937, 168375 (2023).
86. M.H. Phan, New Research Trends in Electrically Tunable 2D van der Waals Magnetic Materials, *Progress in Materials Science* 2023.

87. H.Y. Liu, et al., Enhanced Valley Splitting in Monolayer WSe₂ by Phase Engineering, *ACS Nano* 15, 8244 (2021).
88. W. Hu et al., Synergetic Effect of Substitutional Dopants and Sulfur Vacancy in Modulating the Ferromagnetism of MoS₂ Nanosheets, *ACS Appl. Mater. Interfaces* 2019, 11, 34, 31155–31161
89. W.S. Yun and J. D. Lee, Strain-Induced Magnetism in Single-Layer MoS₂: Origin and Manipulation, *J. Phys. Chem. C* 119, 2822 (2015).
90. V. Ortiz Jimenez, Light-Controlled Magnetism and Magnetic Sensing in Two-Dimensional Vanadium Dichalcogenides and Related Semiconductors, PhD dissertation, 2022.
91. V. Kalappattil, R. Geng, R. Das, M. Pham, H. Luong, T. Nguyen, A. Popescu, L.M. Woods, M. Kläui, H. Srikanth, and M.H. Phan, Giant spin Seebeck effect through an interface organic semiconductor, *Mater. Horizons*. 7, 1413 (2020).
92. Liu, B. et al. Light-Tunable Ferromagnetism in Atomically Thin Fe₃GeTe₂ Driven by Femtosecond Laser Pulse. *Physical Review Letters* 125, 267205 (2020).
93. J. Xie et al., Light Control of Ferromagnetism in ZnO Films on Pt Substrate at Room Temperature, *Scientific Reports* 7, 1–9 (2017).
94. Afanasiev, D. et al. Controlling the anisotropy of a van der Waals antiferromagnet with light. *Science Advances* 7, 1–8 (2021).
95. He, J., Li, S., Bandyopadhyay, A. & Frauenheim, T. Unravelling Photoinduced Interlayer Spin Transfer Dynamics in Two-Dimensional Nonmagnetic-Ferromagnetic van der Waals Heterostructures. *Nano Letters* 21, 3237 (2021).
96. Náfrádi, B. et al. Tuning ferromagnetism at room temperature by visible light. *Proceedings of the National Academy of Sciences of the United States of America* 117, 6417–6423 (2020).
97. Zhou, G. et al. Light-Controlled Ferromagnetism in Porphyrin Functionalized Ultrathin FeS Nanosheets, *Advanced Optical Materials* 8, 1–6 (2020).

98. T.G. Park et al., Interlayer Coupling and Ultrafast Hot Electron Transfer Dynamics in Metallic VSe₂/Graphene van der Waals Heterostructures, *ACS Nano* 15, 4, 7756–7764 (2021)
99. X. Wang et al., Light-induced ferromagnetism in moiré superlattices, *Nature* 604, 468 (2022).
100. C.H. Bao, Light-induced emergent phenomena in 2D materials and topological materials, *Nature Reviews* 4, 33 (2022).
101. X. Chen et al., Generation and Control of Terahertz Spin Currents in Topology-Induced 2D Ferromagnetic Fe₃GeTe₂/Bi₂Te₃ Heterostructures, *Advanced Materials* 34, 2106172 (2022).
102. A. Kimel et al., The 2022 magneto-optics roadmap, *J. Phys. D: Appl. Phys.* 55, 463003 (2022).
103. T.S. Lan et al., Magneto-optic effect of two-dimensional materials and related applications, *Nano Select* 1, 298 (2020).
104. O. Thiabgoh, T.E ggers, and M.H. Phan, A new contactless magneto-LC resonance technology for real-time respiratory motion monitoring. *Sensors and Actuators, A: Physical* 265, 120 (2017).
105. V.O. Jimenez, V. Kalappattil, T. Eggers, M. Bonilla, S. Kolekar, P. T. Huy, M. Batzill, M.H. Phan, A magnetic sensor using a 2D van der Waals ferromagnetic material, *Scientific Reports* 10, 4789 (2020).
106. M.H. Phan, H.X. Peng, Giant Magnetoimpedance Materials: Fundamentals and Applications, *Prog. Mater. Sci.* 53, 323-420 (2008).
107. V. O. Jimenez, K. Y. Hwang, D. Nguyen, Y. Rahman, C. Albrecht, B. Senator, O. Thiabgoh, J. Devkota, V. D. A. Bui, D. S. Lam, T. Eggers, M.H. Phan, Magnetoimpedance Biosensors and Real-Time Healthcare Monitors: Progress, Opportunities, and Challenges, *Biosensors* 12, 517 (2022).

108. F.X. Qin, H. X. Peng, M.H. Phan, L. V. Panina, M. Ipatov, V. Zhukova, A. Zhukov, J. Gonzalez, Novel magnetic microwires-embedded composites for structural health monitoring applications, *J. Appl. Phys.* 107, 09A314 (2010).
109. D. Thi-Xuan Dang, R.K. Barik, M.H. Phan, L.M. Woods, Enhanced Magnetism in Heterostructures with Transition-Metal Dichalcogenide Monolayers, *J. Phys. Chem. Lett.* 13, 8879 (2022).
110. H. Munekata et al., Light-induced ferromagnetism in III-V-based diluted magnetic semiconductor heterostructures magnetic. *Journal of Applied Physics* 81, 4862 (1997).
111. B. Marfouaa and J. Hong, Electric field-induced switching of anomalous Nernst conductivity in the 2D MoTe₂/VSe₂ heterostructure, *Phys. Chem. Chem. Phys.* 24, 22523 (2022).
112. Q. Li, C.X. Zhang, D. Wang, K.Q. Chen, and L.M. Tang, Giant valley splitting in a MoTe₂/MnSe₂ van der Waals heterostructure with room-temperature ferromagnetism, *Mater. Adv.* 3, 2927 (2022).
113. J. Du et al., Two-dimensional transition-metal dichalcogenides-based ferromagnetic van der Waals heterostructures, *Nanoscale* 9, 17585 (2017).
114. C. Freysoldt, B. Grabowski, T. Hickel, J. Neugebauer, G. Kresse, A. Janotti, and C. G. Van de Walle, First-principles calculations for point defects in solids, *Rev. Mod. Phys.* 86, 253 (2014).
115. J. Heyd, G. E. Scuseria, and M. Ernzerhof, Hybrid functionals based on a screened Coulomb potential, *J. Chem. Phys.* 118, 8207–8215 (2003).
116. G. Kresse and J. Furthmüller, Efficient iterative schemes for ab initio total-energy calculations using a plane-wave basis set, *Phys. Rev. B* 54, 11169–11186 (1996).

117. S. Grimme, S. Ehrlich, and L. Goerigk, Effect of the damping function in dispersion corrected density functional theory, *J. Comp. Chem.* 32, 1456 (2011).
118. C. Freysoldt and J. Neugebauer, First-principles calculations for charged defects at surfaces, interfaces, and two-dimensional materials in the presence of electric fields, *Phys. Rev. B* 97, 205425 (2018).
119. N.L. Nair, Maniv, E., John, C. et al. Electrical switching in a magnetically intercalated transition metal dichalcogenide. *Nat. Mater.* 19, 153 (2020).
120. T.S. Ghiasi et al., Charge-to-Spin Conversion by the Rashba–Edelstein Effect in TwoDimensional van der Waals Hetrostructures up to Room Temperature, *Nano Lett.* 19, 5959 (2019).
121. K. Uchida, S. Takahashi, K. Harii, J. Ieda, W. Koshibae, K. Ando, S. Maekawa, E. Saitoh, Observation of the spin Seebeck effect, *Nature.* 455, 778 (2008).
122. K. Uchida, Transport phenomena in spin caloritronics, *Proc. Japan Acad. Ser. B.* 97, 69 (2021).
123. S. Lee, W. Lee, T. Kikkawa, C.T. Le, M. Kang, G. Kim, A.D. Nguyen, Y.S. Kim, N. Park, E. Saitoh, Enhanced Spin Seebeck Effect in Monolayer Tungsten Diselenide Due to Strong Spin Current Injection at Interface, *Adv. Funct. Mater.* 30, 2003192 (2020).
124. J.R. Schaibley, et al., Valleytronics in 2D materials, *Nature Reviews Materials* 1, 16055 (2016).
125. H. Yu, W. Yao, Valleytronics: magnetization without polarization. *Nat. Mater.* 16, 876 (2017).
126. G. Aivazian, Z. Gong, A.M. Jones, R.-L. Chu, J. Yan, D.G. Mandrus, C. Zhang, D. Cobden, W. Yao, X. Xu, Magnetic control of valley pseudospin in monolayer WSe₂, *Nat. Phys.* 11, 148 (2015).

127. T. Norden, C. Zhao, P. Zhang, R. Sabirianov, A. Petrou, H. Zeng, Giant valley splitting in monolayer WS₂ by magnetic proximity effect, *Nat. Commun.* 10, 1–10 (2019).
128. J.J. He et al., Ultrafast Light-Induced Ferromagnetic State in Transition Metal Dichalcogenides Monolayers, *J. Phys. Chem. Lett.* 13, 2765 (2022).
129. A.V. Kimel and M. Li, Writing magnetic memory with ultrashort light pulses, *Nature Reviews* 4, 189 (2019).
130. Y. Li, M. Koshino, Twist-angle dependence of the proximity spin-orbit coupling in graphene on transition-metal dichalcogenides. *Phys. Rev. B* 99, 075438 (2019).
131. A. David, Induced spin-orbit coupling in twisted graphene–transition metal dichalcogenide heterobilayers: twistronics meets spintronics. *Phys. Rev. B* 100, 085412 (2019).
132. S.J. Lee, D. J. P. de Sousa, Y.K. Kwon, F. de Juan, Z.D. Chi, F. Casanova, and T. Low, Charge-to-spin conversion in twisted graphene/WSe₂ heterostructures, *Phys. Rev. B* 106, 165420 (2022).
133. N. Ontoso, C. K. Safeer, Franz Herling, Josep Ingla-Aynés, Haozhe Yang, Zhendong Chi, Beatriz Martin-Garcia, Iñigo Robredo, Maia G. Vergniory, Fernando de Juan, M. Reyes Calvo, Luis E. Hueso, and Fèlix Casanova, Unconventional Charge-to-Spin Conversion in Graphene/MoTe₂ van der Waals Heterostructures, *Phys. Rev. Applied* 19, 014053 (2023).
134. J.X. Lin et al., Spin-orbit–driven ferromagnetism at half moiré filling in magic-angle twisted bilayer graphene, *Science* 375, 437 (2022).
135. H. Yang et al., Advance in two-dimensional twisted moiré materials: Fabrication, properties, and applications, *Nano Res.* 16, 2579 (2023).
136. X. Sui et al., Voltage-controllable colossal magnetocrystalline anisotropy in single-layer transition metal dichalcogenides. *Phys. Rev. B* 96, 041410 (2017).

137. X.G. Liu, et al., Magnetoelectric Coupling in Multiferroic Bilayer VS₂, PRL 125, 247601 (2020).
138. H.C. Bouzid et al., Enhanced magnetic moment with cobalt dopant in SnS₂ semiconductor, APL Mater. 9, 051106 (2021).
139. B. Li et al., A two-dimensional Fe-doped SnS₂ magnetic semiconductor, Nature Communications 8, 1958 (2017).
140. H.C. Bouzid et al., Multiple Magnetic Phases in Van Der Waals Mn-Doped SnS₂ Semiconductor, Adv. Funct. Mater. 31, 2102560 (2021).